Available online at www.sciencedirect.com
ScienceDirect
Earth and Planetary Science Letters 256 (2007) 100–119
EPSL
www.elsevier.com/locate/epsl

Transient mantle convection on Venus: The paradoxical coexistence of highlands and coronae in the BAT region

Catherine M.I. Robin [a,*], A. Mark Jellinek [b], Vid Thayalan [c], Adrian Lenardic [d]

[a] Departments of Physics and Geology, University of Toronto, Toronto, ON, Canada
[b] Department of Earth and Ocean Sciences, University of British Columbia, Vancouver, BC, Canada
[c] Department of Earth, Atmospheric and Planetary Sciences, Massachusetts Institute of Technology, Boston, MA, USA
[d] Department of Earth Science, Rice University, Houston, TX, USA

Received 25 April 2006; received in revised form 5 January 2007; accepted 11 January 2007
Available online 19 January 2007
Editor: S. King

Abstract

The coexistence of Venusian highlands, attributed to long-lived axisymmetric mantle plumes, and uncompensated coronae, attributed to transient discrete mantle 'thermals', is difficult to reconcile with models of mantle convection under thermally steady-state conditions. However, cratering and geological studies indicate a uniformly young surface age (~ 700 Myr) as well as a comparable timescale for resurfacing (~ 100 to 400 Myr), possibly consistent with a recent lithospheric overturn and a transient mantle thermal regime. We use laboratory experiments on free and forced thermal convection at high Rayleigh number ($Ra \sim 10^7$) in a variable viscosity fluid to investigate the steady-state and transient thermal regimes preceding and following such an overturn. From analyses of shadowgraph images and time series of global and local variations in temperature, basal heat flux and viscosity, we establish steady-state stagnant- and active-lid states and characterize two intermediate transient regimes. Flow in steady-state stagnant lid is in the form of intermittent thermals, consistent with published work. During the transition to active-lid convection the stagnant lid is stirred into the interior using a conveyor belt. Spreading of this cold fluid along the hot boundary leads to a transition to a "mixed mode" of flow from the hot boundary: approximately isoviscous thermals rise from the thermal boundary layer ahead of the advancing cold front and low viscosity plumes rise from behind the front, as a result of an enhanced temperature contrast. The longevity of this regime and the timescale for the transient depends on the rate of overturn (Pe) and the aspect ratio of the system (A). The magnitude of local temperature, viscosity and heat flux variations increases with Pe and can exceed steady-state values for active-lid convection. Additional numerical simulations show that the mixed mode regime will occur in the presence of internal heating, and for no- and free-slip boundaries. In contrast, the transition from active-lid to stagnant-lid convection is marked by a change from a flow composed of plumes and large-scale overturning motions to a regime dominated by rising and sinking thermals on a timescale of thermal diffusion. Applied to Venus, our results support a hypothesis that the contemporaneous coexistence of the Atla and Beta highlands regions with interspersed uncompensated coronae is consistent with a transient thermal regime following a lithospheric overturn. It is also expected that such coronae formed > 250 Myr after the uplift of the highlands. Implications of the thermal origin of coronae for Venusian mantle structure are also explored.

Keywords: transient mantle convection; Venus; coronae; highlands; mantle thermals and mantle plumes

* Corresponding author. Tel.: +1 416 978 5177; fax: +1 416 978 7606.
E-mail address: crobin@physics.utoronto.ca (C.M.I. Robin).

0012-821X/$ - see front matter © 2007 Elsevier B.V. All rights reserved.
doi:10.1016/j.epsl.2007.01.016

1. Introduction

Among the most intriguing classes of topographic features on Venus are approximately 500 quasi-circular coronae [1–3]. Coronae are typically ~ 250 km in diameter [3,4] and are concentrated in a large triangular region bounded by the highlands Atla, Beta and Themis (known as the BAT region) (Fig. 1a) [1,5]. Interpretations of the axisymmetric shapes of coronae, combined with their association with a broad variety of volcanic and tectonic features [1,6–8] have contributed to a general picture that they are, directly or indirectly, related to transient upwellings from the upper mantle or the core–mantle boundary (CMB) (e.g. [5,9–12]), the nature and origin of which remain an area of active research [5,7,13–18]. In contrast, the BAT highlands themselves are generally thought to reflect continuous and strong upwelling flow in the mantle. This picture stems from considerations of a combination of large volcanic constructs on each of the highlands (e.g. [7]) as well as strong axisymmetric geoid highs analogous to those observed over Hawaii [19].

In a recent paper, Johnson and Richards [5] analyze the statistical distribution of coronae characterized by positive gravity anomalies, plausibly explained by dynamic support from upwelling flow in the mantle. These authors find that whereas the majority of these "uncompensated" features are concentrated within the BAT region, the distribution of compensated coronae is relatively insensitive to geographical region. From the geometric relationship between the BAT highlands and uncompensated BAT coronae, along with inferences drawn from the results of laboratory experiments on mantle convection (e.g. [20–22]), Johnson and Richards [5] develop a conceptual model for a "mixed-mode" style of Venusian mantle convection that explains the temporal coexistence of coronae and the highlands (Fig. 1b). In particular, Johnson and Richards [5] envision that mantle convection driven by heat transfer from Venus' core is in a regime characterized by two types of upwelling. Approximately steady flow in long-lived narrow axisymmetric conduits, akin to the style of flow often inferred to occur within mantle plume conduits (i.e. "tails") in the Earth (e.g. [23–25]), gives rise to the highlands (see discussions in [26,27]). In contrast, transient mantle thermals [28–30] are suggested to explain coronae [20,21]. (A more complete discussion of the conditions that give rise to mantle plumes and thermals can be found in [31]).

The Johnson and Richards [5] model is consistent with available geophysical and volcanological constraints and elegantly explains the coexistence of coronae and the highlands. However, while the model is plausible, the inferred large lateral variations in the style of mantle upwelling flow present a difficult conundrum for existing geodynamic models of mantle convection. In particular, whereas long-lived, axisymmetric plume conduits are thought to be characteristic of upwellings that are greater than one or two orders of magnitude less viscous than surrounding mantle [23,24,31–36], transient thermals are typical of flows in which the viscosity variations are order unity [21,37,38]. In addition, under thermally steady-state conditions a number of studies have implied or shown that the conditions leading to either upwellings in the form of thermals or upwellings in the form of low viscosity plumes are distinct and highly restrictive [31,39,40] and thus it is unclear how two such regimes may occur together at the same time. For example, approximately isoviscous thermals are expected to form if the internal mantle temperature is close to that of the core–mantle boundary, a characteristic of stagnant-lid convection expected to occur in a one-plate planet [41,42]. In contrast, the large temperature variations in the hot thermal boundary layer that can give rise to low viscosity plume conduits may arise only in an "active lid" regime characterized by subduction and large-scale stirring of the cold lithosphere [31,34,43]. Thus, to explain the coexistence of uncompensated BAT coronae and the Atla and Beta regions with a "mixed-mode" model (Fig. 1b) an essential issue is to establish the origin of large lateral differences in the temperature drop across the thermal boundary layer at the core–mantle boundary of Venus.

It is important to realize that the spatial and temporal coexistence of thermal regimes giving rise to contemporaneous low viscosity mantle plumes and isoviscous mantle thermals is problematic if and only if Venus is currently in a thermally steady-state regime. Indeed, it is unclear whether it is reasonable to expect such a condition. Constraints on the mean surface age derived principally from cratering studies [44–46] are consistent with an average age of only 700–800 Myr. In addition, the results of detailed analyses of the local statistics of cratering populations [47] and recent geological mapping [8,48] are collectively consistent with either a rapid (~100 Myr) or more gradual (>400 Myr) global resurfacing of the planet. Explanations of the nearly uniform and young surface age have been presented in terms of a catastrophic overturn of the Venusian lithosphere followed by little resurfacing thereafter (e.g. [45,49–52]), a more "gradual" resurfacing [48], and the outward expression of an episodic style of plate tectonics [51–54]. Although the timescale and style for resurfacing is poorly constrained, the fundamental transition in tectonic regime to a current one-plate state beginning about 700–800 Myr ago is undisputed. If the resurfacing is related to

a foundering of the lithosphere occurring on a timescale of 100–400 Myr then it is reasonable to hypothesize the Venusian mantle to be currently adjusting to a new thermal condition [e.g. [55]]. Consequently, in this paper we use laboratory experiments supported by a small suite of numerical simulations to explore in detail the transient regime of mantle convection that may follow an overturn of the lithosphere. We also investigate the transient regime following the cessation of forced large-scale stirring. In addition to characterizing these regimes our goal is to identify whether it is reasonable to expect such a mixed-mode of convection, as described in Fig. 1b, in the mantle of Venus following a lithospheric overturn.

2. Laboratory experiments

2.1. Apparatus and method

Our convection experiments are performed in the 30 cm × 33 cm × 22.5 cm tank shown in Fig. 2. The

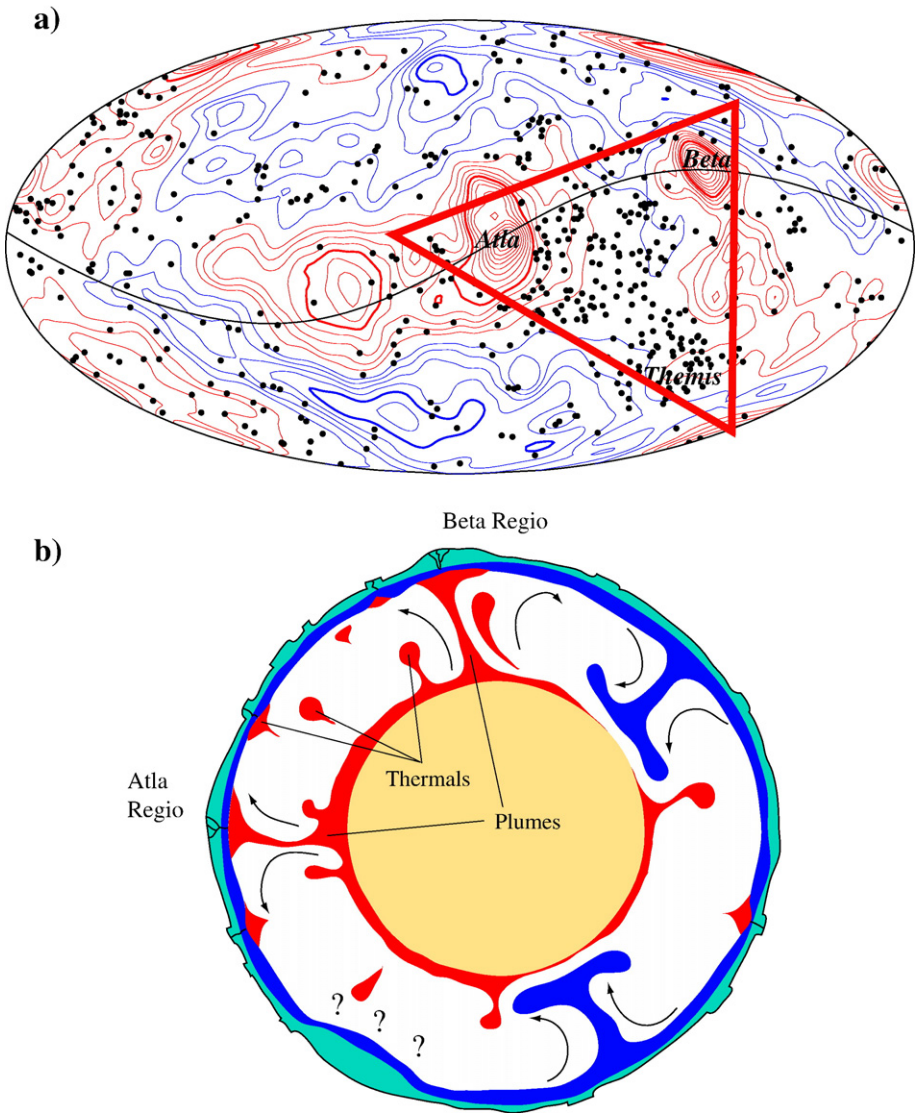

Fig. 1. a) Corona distribution superposed on a map of the Venus geoid modified from Johnson and Richards [5]. Coronae are concentrated within a triangular area bound by the Beta–Atla–Themis (BAT) highland regions (red triangle). Beta and Atla are characterized by strong, axisymmetric positive geoid anomalies, consistent with dynamic support from mantle upwelling. b) A conceptual model for a "mixed-mode" style of Venusian mantle convection proposed by Johnson and Richards [5] to explain the coexistence of dynamically-supported coronae (principally within the BAT region) and the highlands themselves. Whereas coronae are proposed to be the surface expression of transient thermals, the highlands are better explained in terms continuous axisymmetric mantle upwellings. See text.

sidewalls are insulated plexiglass. The upper (cold) and lower (hot) boundaries are aluminum heat exchangers through which cold and hot water is pumped at a high rate, such that isothermal boundary conditions, characteristic of Rayleigh–Benard convection, are achieved. Our working fluid is ADM 36/43 corn syrup, which has a viscosity that depends strongly on temperature (Table 1). Submerged a few millimeters below the cold boundary is a 2 mm thick motor-controlled "conveyor" belt constructed of reinforced neoprene that is used to drive a tank-filling large-scale flow. The belt is extensively drilled with 1 cm diameter holes to maximize thermal contact with the roof heat exchanger.

At the start of each experiment, boundary temperatures are set such that the system evolves to a regime of steady-state stagnant-lid convection at high-Rayleigh number that is quantitatively similar to previous studies (e.g. [30,38]) (Fig. 2b, Table 2). A statistical steady-state is indicated by constant and equal heat fluxes at the cold and hot boundaries and a well-defined mean internal temperature that does not vary in time. We note that the belt is positioned near the top of the stagnant part of the cold thermal boundary layer and thus does not influence the flow in this regime [56]. Once this basic state is established the conveyor belt is turned on at a fixed velocity that we vary. Resultant large-scale flow overturns and stirs the cold thermal boundary layer into the underlying fluid, and forces an active-lid style of convection [53] (Fig. 2b). Where possible the belt is driven until thermally steady-state conditions are

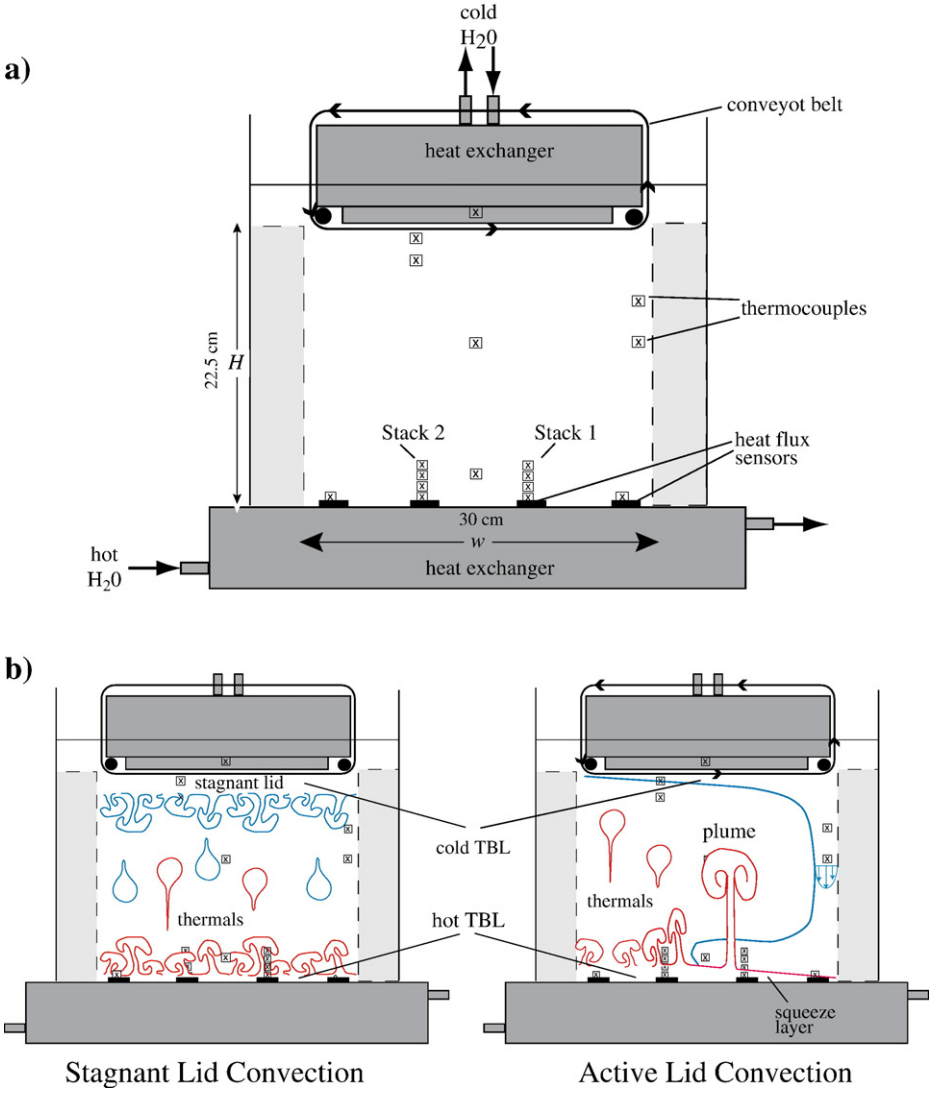

Fig. 2. a) A schematic diagram of the experimental apparatus. b) Cartoons showing stagnant-lid and (forced) active-lid convection in our experiments.

Table 1
Physical properties

Parameter	Symbol	Value
Coefficient of thermal expansion of syrup*	α	5.61×10^{-4} °C^{-1}
Density of syrup*	ρ	$\rho(T)=10^3(-5.60774\times10^{-4}T+1.46201)$ kg/m^3
Dynamic viscosity of syrup**	μ	$\mu(T)=\exp(6.7057-0.1353T+0.0004T^2)$ Pa s
Gravitational acceleration	g	9.81 m/s^2
Thermal conductivity of syrup*	K	$K(T)=0.365+0.00245T$ W/m/°C
Thermal diffusivity of syrup*	κ	1×10^{-7} m^2/s

* from Jellinek et al., 2003 [56].
** measured in our laboratory.

achieved. However, the large viscous stresses involved in stirring the cold lid into the underlying fluid make the experiments technically difficult, and ultimately limit the range of parameter space we are able to investigate (Table 2).

Experiments are quantified using time series of temperature and local heat flux. Local heat flux is measured using four Omega HFS4 heat flux sensors distributed across the hot boundary (Fig. 2). Wire thermocouples are located along the hot, cold and sidewall boundaries, and in the interior of the system. To characterize the local vertical and lateral temperature and viscosity variations in the hot thermal boundary layer in both transient and steady-state regimes, as well as the corresponding local heat fluxes, we apply thermocouple stacks above two heat flux sensors (referred to as "stack 1" and "stack 2"). *Stack 1* and *stack 2* are constructed of 4 to 6 J-type thermocouples spaced 0.5 to 1 cm apart, designed to record the downstream evolution of the hot thermal boundary layer occurring in response to the forced spreading cold material. In addition, the qualitative structure of all flows is characterized using a combination of time-lapse and still photographs of shadowgraphs, which capture fluid motions by mapping vertical and lateral variations in refractive index that occur with corresponding changes in temperature.

2.2. Dimensionless parameters

Five dimensionless parameters characterize our experiments. The aspect ratio, $A=H/w=1.3$, is constant. All experiments are conducted at high Prandtl number, ($Pr=\mu/\rho\kappa\geq10^4$) such that the Reynolds number for all experiments is less than about unity and inertial effects may be neglected. Here, μ is viscosity, ρ is density, κ is thermal diffusivity, H is the layer depth and w is the tank width (Table 1). The vigour of buoyancy-driven motions is characterized by the Rayleigh number,

$$Ra=\frac{g\rho_i\alpha\Delta TH^3}{\mu_i\kappa} \quad (1)$$

where μ_i is the viscosity based on an appropriate mean interior temperature (Table 2), ΔT is the temperature drop from the hot boundary to the cold boundary, g is gravity and α is the coefficient of thermal expansion. The velocity of the imposed circulation is varied for each experiment and is expressed with a Peclet number,

$$Pe=\frac{VH}{\kappa}, \quad (2)$$

where V is the belt velocity. The magnitude of the total viscosity variations in the system is given by the total viscosity ratio,

$$\lambda_t=\frac{\mu_c}{\mu_h}, \quad (3)$$

where the subscripts "c" and "h" denote parameters measured at the cold and hot boundaries. All of our experiments are conducted under approximately

Table 2
Properties of 5 experiments discussed in the text

Run	Regime	Ra	Pe	λ_i^*	λ_t^*	θ	q^* (W/m^2)
14	Stagnant lid	5.4×10^7	–	4	4	.75	980
	Transient I	2.9×10^7	9100	15	19	.61	2400
	Active lid	2×10^7	9100	11	17	.60	2000
15	Stagnant lid	5.2×10^7	–	4	4	.74	970
	Transient I	3×10^7	23,000	12	22	.66	2000
	Active lid	2.6×10^7	23,000	8	19	.63	1100
17	Stagnant lid	1.1×10^8	–	4	5	.78	1300
	Transient	8.6×10^7	4500	8	13	.75	2900
	Active lid	5.7×10^7	4500	7	12	.66	2100
18	Stagnant lid	3.3×10^8	–	4	4	.79	1200
	Transient I	3.2×10^7	2300	4	6	–	2700
	Active lid	–	2300	–	–	–	–
19	Stagnant lid	2.8×10^7	–	4	4	.75	1200
	Transient I	2.6×10^7	31,000	–	35	–	3300
	Active lid	–	31,000	–	–	–	–

All transient flows are complex and properties are based on measurements made at stack 1 and stack 2 (Fig. 2). In cases where there are no values reported for the transient or active-lid regimes we could not maintain a fixed velocity condition at the to surface for sufficient time to obtain a reliable measurement. See text.
* is the maximum during the transient, and the mean for stagnant- and active-lid. Other values represent means.

constant and high Ra ($>10^7$) conditions (Table 2). In addition, $\lambda_t \sim 10^3$, such that the convection is in the stagnant-lid regime when $Pe=0$ [21,30].

Along with these external parameters it will be useful to introduce some additional parameters determined internally. We define internal temperature, $\theta=(T_i-T_c)/(T_h-T_c)$ and the hot boundary layer viscosity ratio, $\lambda_h^*=\mu_i^*/\mu_h$. Because we are interested in transient phenomena, which may not be global in scale, λ_h^* is a local viscosity ratio, where the superscript "*" indicates values based on the maximum temperature differences recorded at *stack 1* and *stack 2*. For the same reason, we define a local heat flux ratio q^*, which is the measured convective heat flux, q, normalized to the average steady-state stagnant-lid heat flux, q^s. We also define the local internal temperature normalized to the stagnant-lid value, $\theta_i^*=(T_i^*-T_c)/(T_i^s-T_c)$, where the superscript "s" denotes "stagnant lid". Under statistically steady-state conditions these local parameters are equivalent to the global values.

3. Experimental results

In Table 2 we present results from 5 experiments from a larger series of 21 runs. In particular, we identify and characterize two transient thermal regimes. The first (transient 1) occurs when the belt is turned on, and the system is forced to evolve from steady-state stagnant-lid convection towards steady-state convection in the active-lid regime. The second (transient 2) occurs when the belt is turned off, and the system returns from steady-state active-lid convection towards a fully developed stagnant-lid regime. Owing to practical difficulties involved with

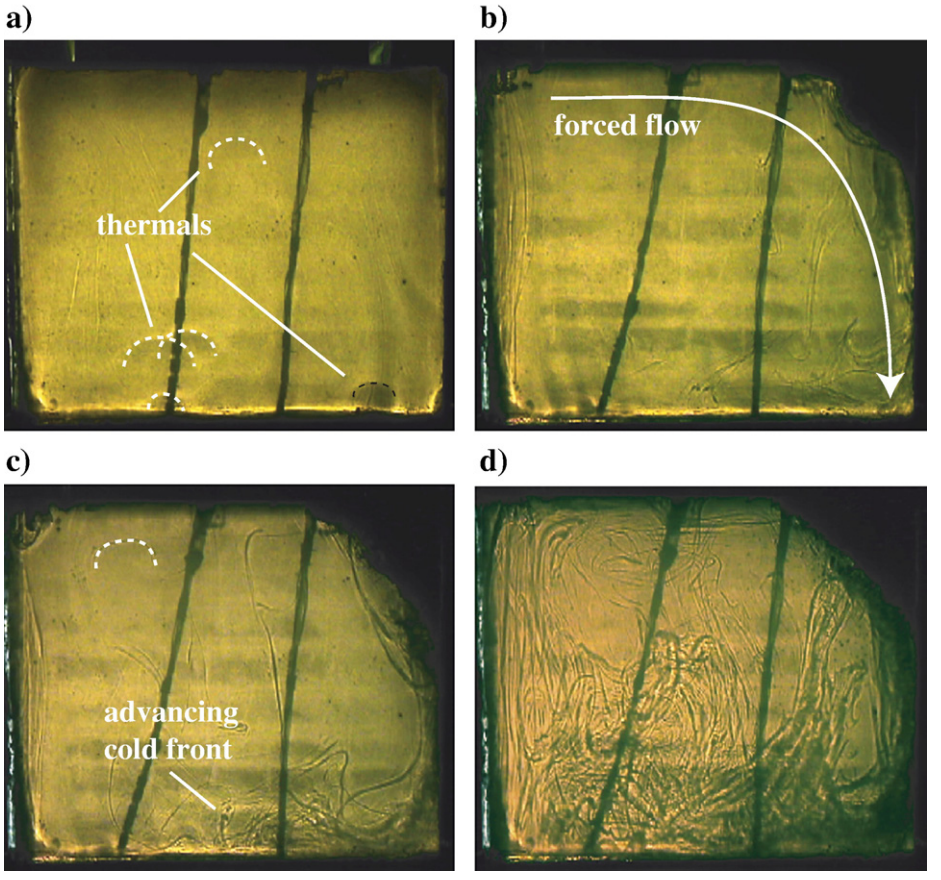

Fig. 3. Shadowgraph images showing the evolution of the system away from a stagnant-lid regime following initiation of forced stirring from above. a) Steady-state stagnant-lid convection in which upwellings are transient thermals. Transient cold downwellings are not observed in this image but are apparent in time series of temperature. b) The conveyor belt at the cold boundary is turned on, resulting in a forced advection of the cold stagnant lid down the sidewall to the floor of the tank. c), d) Cold fluid spreads across the floor and is stirred into the fluid interior. $Ra=1.1\times10^8$, $Pe=4500$, $\lambda_t\approx10^3$.

achieving steady-state active-lid convection over a range of *Pe* conditions our discussion of this regime is limited to its qualitative features.

3.1. Qualitative results

3.1.1. Transient 1: stagnant-lid to active-lid convection

Figs. 3 and 4 are time series of shadowgraph images characterizing the transition away from a stagnant-lid regime as the cold boundary layer is stirred into the underlying fluid through one complete overturn. In Fig. 3a, $Pe=0$ and the flow is in the stagnant-lid regime under statistically steady-state conditions. Convection is in the form of intermittent rising and sinking thermals. The internal temperature, $\theta=0.76$, and the viscosity ratio, $\lambda_h=4$ (i.e. order 1), which are quantitatively consistent with previous studies [20,21,30,38]. The very small refractive index contrast between the upwelling thermals and colder fluid interior is indicative of the small temperature difference that corresponds with an order 1 viscosity variation [31,38].

Figs. 3b–d and 4 capture the evolution in flow regime after the belt is turned on. Cold and dense fluid, characterized by a high refractive index contrast, is forced down the sidewall and along the hot boundary. Hot thermal boundary layer fluid is, in turn, overrun and "bulldozed" ahead of this advancing front of cold fluid (e.g. [57]) resulting in a thermal boundary layer that thickens monotonically downstream. Local advective thickening of the hot thermal boundary layer directly ahead of the cold front enhances convective instabilities such that frequency of thermal formation is higher than that occurring further downstream (Fig. 4), where the thermal boundary layer grows by vertical thermal diffusion alone. The magnitude of this spatial variation in thermal formation frequency depends on the importance of lateral advection of thermal boundary layer fluid and consequently increases with *Pe*. This is discussed in more detail below.

Hot thermal boundary layer that is overrun by the cold current is trapped as a so-called "squeeze layer" [58]. Further thickening of the squeeze layer by

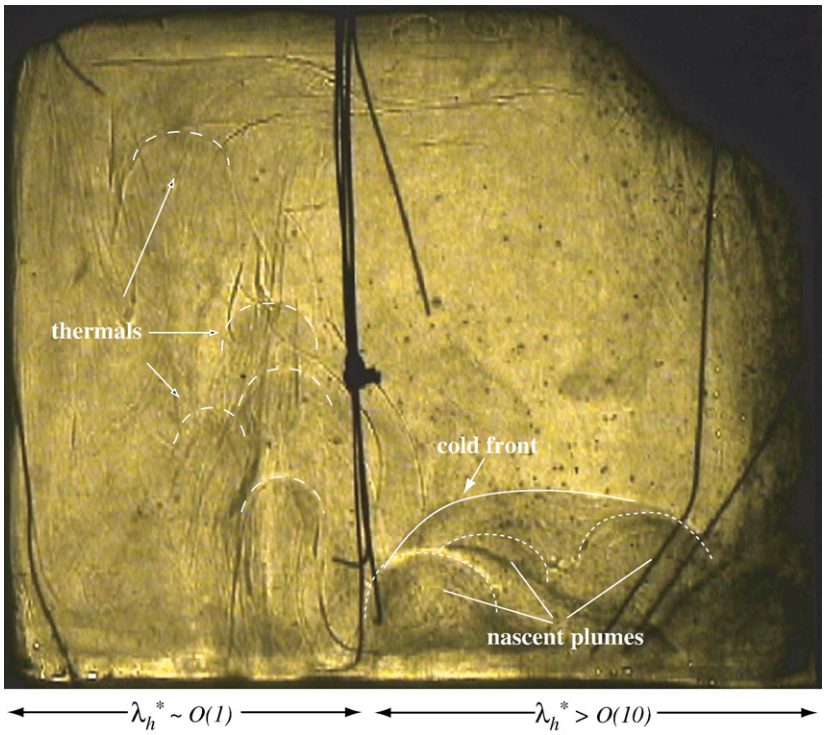

Fig. 4. Shadowgraph showing a snapshot from transient 1. The advancing cold front extends to midway across the tank. Upstream from the cold front, $\lambda_h^*=60$ and nascent low viscosity plume instabilities (large heads) are observed. Downstream from the cold front $\lambda_h^*=4$ and upwellings are thermals. The clustering of thermals near the leading edge of the cold front reflects a higher frequency of thermal formation. This is interpreted to occur because the lateral spreading of cold material causes the hot boundary layer to thicken downstream more rapidly than it would by vertical conduction alone. The ratio of the diameter of low viscosity plume heads to the diameter of thermals scales approximately as $(\lambda_h^*/\lambda_h^s)^{1/3}$, consistent with Rayleigh–Taylor theory. $Ra=1\times10^8$, $Pe\approx28{,}000$, $\lambda_t\approx10^3$.

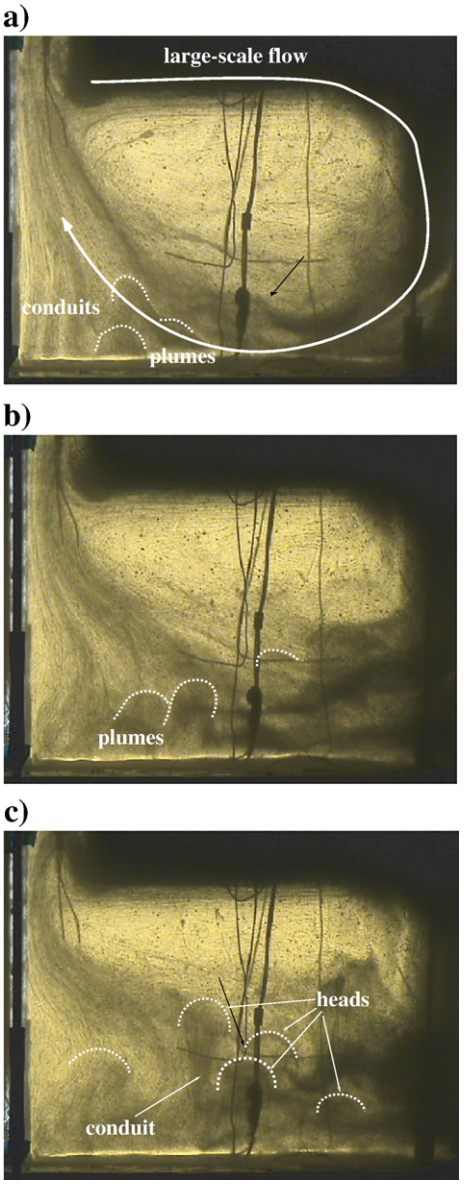

Fig. 5. Shadowgraph images of transient 2: The evolution from steady-state active-lid convection following cessation of the imposed large-scale flow. a) Steady-state active-lid convection. Dark bubbles show the geometry of the imposed motions (white arrow). Rising low viscosity plumes are drawn into the large-scale flow [Jellinek et al., 2003]. Plume conduits are clustered near the left side of the tank. b), c) The belt is turned off and plumes rise more vertically. Heads and trailing conduits are evident in c). $Ra=2\times10^7$ (during steady-state active lid), $Pe=26{,}000$, $\lambda_t\approx10^3$, $\lambda_h\approx16$.

conductive heat transfer from the hot boundary leads to convective instabilities that take the form of low viscosity plumes with large heads and narrow axisymmetric conduit tails rising through the cold layer (Fig. 4) [31,37]. These plume heads are larger in diameter than the thermals forming downstream of the spreading cold fluid. Where possible the ratio of the diameter of the plume heads to the diameter of the thermals was measured as close to the leading edge of the hot boundary layer as possible and found to be proportional to $(l_h^*/\lambda_h^s)^{1/3}$, consistent with expectations from Rayleigh–Taylor theory [23,59–61].

An essential characteristic of this transient regime is that large lateral variations in temperature and viscosity across the hot boundary layer lead to a mixed mode style of flow characterized by a contemporaneous formation of approximately isoviscous thermals and low viscosity plumes in the same flow. However, it is important to note that once the cold material blankets the cold boundary entirely the flow from the hot boundary is in the form of low viscosity plumes only. Thus, in our system the coexistence of these two types of upwelling structures is a characteristic of the early part of this transient regime. More generally, the longevity of this regime depends on the rate at which the cold boundary layer is overturned, *Pe*, and the length of the hot boundary expressed as a function of the aspect ratio, *A*, which we do not vary.

3.1.2. Transient 2: active-lid to stagnant-lid convection

Active-lid convection under thermally steady-state conditions is achieved in only a few cases. An essential difference to the stagnant-lid regime is that the stronger cooling effect of stirring the cold fluid in contact with the top boundary into the underlying fluid interior leads to a lower interior temperature and to larger temperature and viscosity variations in the hot thermal boundary layer. A time series of shadowgraph images illustrating steady-state active-lid convection and the thermal transient following the cessation of the imposed stirring is shown in Fig. 5. Fig. 5a shows a fully developed flow composed of an asymmetrical large-scale flow along with sheared low viscosity plumes ascending from the hot boundary [35,62] (Table 2). Fig. 5b and c shows the transient regime in which the forced flow has ceased and plumes with large heads rise vertically. Because the interior temperature is less than in the stagnant-lid regime, vertically rising plume heads carry a comparatively much greater excess temperatures (indicated in Fig. 5 by the large contrasts in refractive index compared to Fig. 3a), and are significantly less viscous and larger than thermals.

3.2. Quantitative results for transient 1

To characterize the evolution in flow regime as a function of *Pe* through transient 1 we analyze local time

series of temperature, θ_i^*, heat flux, q^*, and the viscosity ratio across the hot thermal boundary layer, λ_h^* acquired from both *stack 1* and *stack 2* (Fig. 2). It is important to note that whereas the stacks capture the hottest temperature in the thermal boundary layer (the hot boundary temperature), by virtue of their design they do not necessarily capture the lowest temperature carried by cold material that advances across the hot boundary. Consequently, our absolute measurements at these locations likely underestimate the effects of the spreading cold front on the local temperature and viscosity variations. However, relative differences between experiments (and between each experiment and the stagnant-lid case) are preserved such that we may characterize and compare flows in a self-consistent way.

3.2.1. Temporal dynamics: frequency of thermal formation

Fig. 6a and b shows time series for the internal temperature for stagnant-lid convection under steady-state conditions along with the corresponding power spectra. Two observations are noteworthy. First, as mentioned above, the mean interior temperature, $\theta \approx 0.76$ and convection is in the form of intermittent thermals expressed as positive temperature anomalies, consistent with previous work [31]. Second, we identify distinct frequencies for the formation of hot and cold thermals in both the hot and cold thermal boundary layers the ratio of which is consistent with that found by Schaeffer and Manga [20].

As outlined above, the spreading of cold fluid along the hot boundary influences the temporal (and spatial) dynamics of the hot boundary layer. To analyze these transient data in the spectral domain we lowpass filter the data and remove the secular trend such that the time series are quasi-stationary. Because frequency resolution is ultimately limited by the number of convective instabilities that can occur during length of the transient it is enhanced for low-*Pe* flows. Nevertheless, comparison of Fig. 6b and c illustrates how the power spectra at *stack 1* evolve in response to the progressive stirring of cold boundary layer material during transient 1 for a run in which $Pe = 23{,}000$.

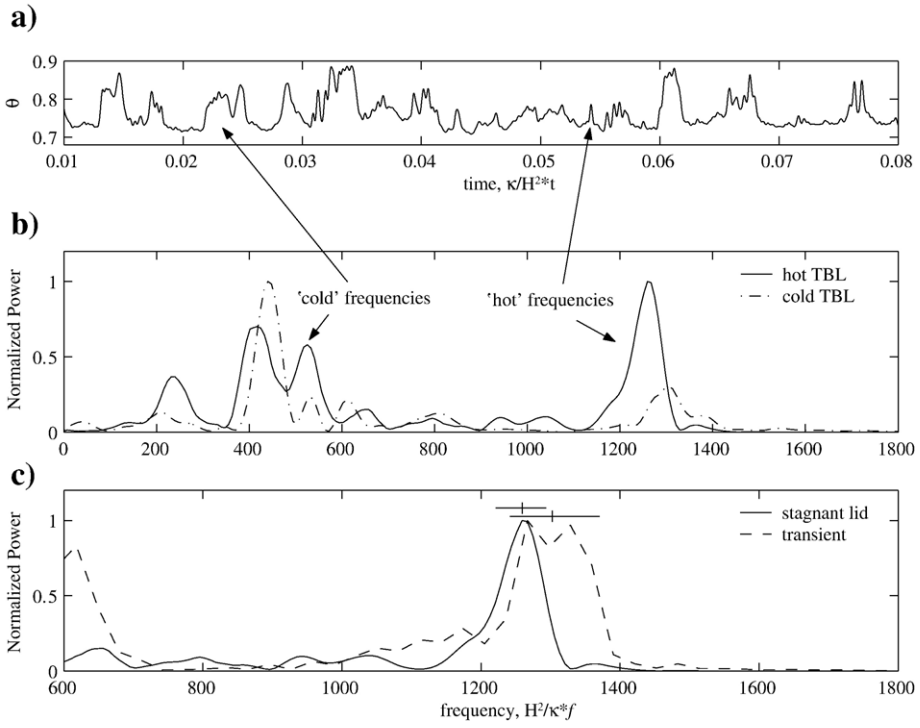

Fig. 6. Plots showing the temporal dynamics of the hot thermal boundary layer during stagnant-lid convection and transient 1. a) Time series of internal temperature for run 15 (Table 2); b) power spectra for the same experiment based on time series of temperature recorded in both the hot TBL (stack 2) and cold TBL during stagnant-lid convection. Frequencies for the formation of hot and cold thermals are found in both boundary layers, indicating that convective instabilities in the hot and cold boundary layers are influenced by sinking (cold) and rising (hot) thermals, respectively [63]. c) Power spectra from a time series of temperature from stack 2 obtained during transient 1. The advection of cold material along the hot boundary causes the frequency of hot thermal formation to increase. See text.

Comparison of the average hot frequency through the transient with that during the stagnant lid suggests that there is a shift to a higher frequency, consistent with the advective thickening of the hot thermal boundary layer discussed above (Fig. 4).

3.2.2. Temperature and viscosity variations

The coexistence of thermals and plumes during transient 1 implies that lateral temperature, and thus viscosity, variations govern the structure of the flow in this regime. Fig. 7 shows the evolution of local temperature variations recorded at *stack 1* and *stack 2* as a function of *Pe* for four experiments. Each experiment begins in the stagnant-lid regime. The belt is then turned on for >1 full overturns. Only the experiments in Fig. 7b, c and d reach steady-state active-lid conditions before the belt is turned off (or the conveyor belt system fails). The internal temperatures under these conditions are $0.60<\theta<0.66$. The interior temperature is greater than 0.5 because the measurements are local values and do not include lateral temperature variations arising due to the cavity-flow structure of the forced large-scale stirring.

Comparison of the data from both stacks characterizes the downstream thermal evolution of the advancing cold material and its influence on the structure of the vertical and lateral temperature variations within the thermal boundary layer. Following the onset of stirring the average and maximum cold temperatures decline from the stagnant-lid values as the temperature drop from the hot boundary increases. Both the cooling of the thermal boundary layer and the vertical temperature gradients across each stack are maximized for the largest *Pe* (Fig. 7a). In addition, the local internal temperature is lower at *stack 2* than at *stack 1* because the cold front warms as it spreads across the hot boundary. For more moderate *Pe* (Fig. 7b, c) the internal temperature declines to a minimum value, where it remains. For the lowest *Pe* experiment (Fig. 7d) there is little difference to the stagnant-lid case.

Fig. 8 shows the local variations in λ_h^* that correspond to the temperature variations in Fig. 7. As for temperatures, viscosity ratio increases when the belt is turned on, and is maximized for large *Pe*. Whereas for $Pe=23{,}000$, a nearly 6-fold increase in λ_h^* is observed, little variation compared with the stagnant-lid case is

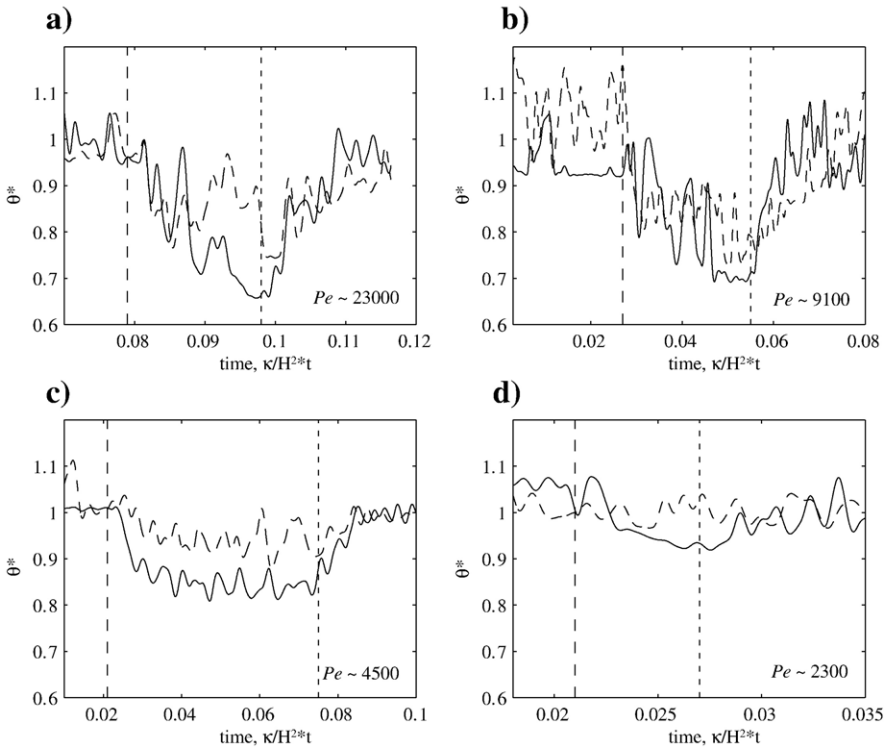

Fig. 7. Local temperature variations in the hot TBL at stack 2 (solid lines) and stack 1 (dashed lines) for different *Pe* (runs 15, 14, 17 and 18 in Table 2), normalized to the average θ_σ during steady-state stagnant-lid convection. The vertical lines mark the time when the belt is turned on (long dashes) and turned off (short dashes). ΔT across the hot thermal boundary layer was measured 4 cm above the hot boundary in stack 1 and stack 2. Since the position of these thermocouples was fixed, they may not have captured the full extent of the temperature difference across the hot TBL.

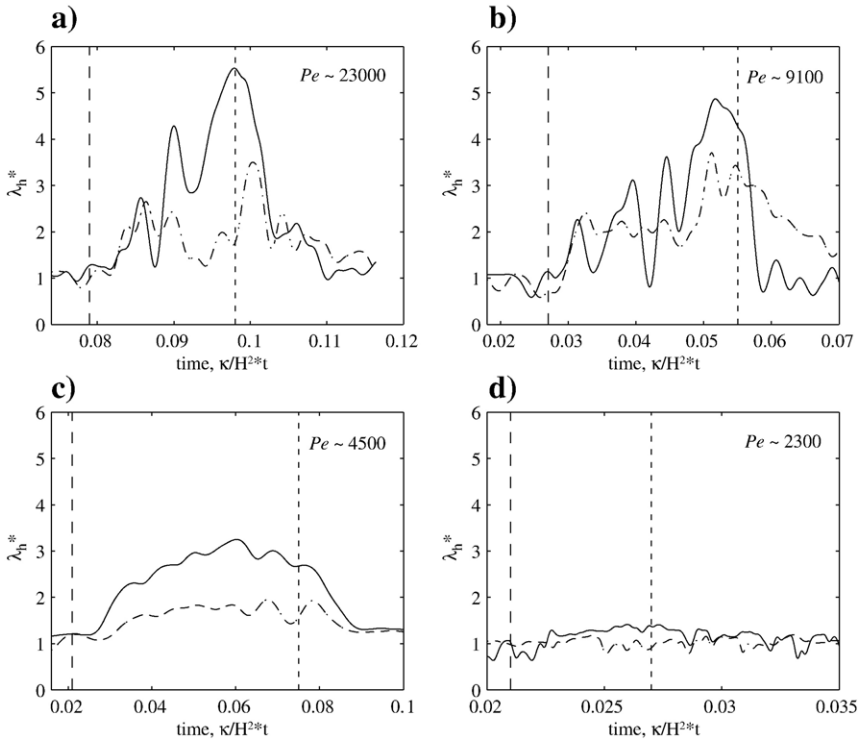

Fig. 8. Plot of local viscosity ratios measured at stack 2, normalized to the average λ_s during stagnant-lid convection for different *Pe*. Plot parameters are the same as in Fig. 7. See text for discussion.

recorded for $Pe \sim 2300$. We note that the 6-fold increase in λ_h^* is around a factor of 1.5 smaller than that which would be obtained from comparison of the ratio of plume to thermal head sizes (Section 3.1.1) and the discrepancy is due to the way in which stack 2 samples the vertical temperature field.

3.2.3. Local heat flux

Fig. 9 shows local heat flux measured beneath *stack 2* as a function of *Pe* for five experiments. At the start of the transient q^* increases linearly from 1 to a maximum, the magnitude of which increases with *Pe*. Subsequently, q^* declines from this maximum and in some cases recovers a constant and lower value characteristic of steady-state active-lid convection. Following cessation of the forced stirring q^* decreases from the to a steady-state stagnant-lid value at a rate approximately proportional to $t^{1/2}$, consistent with a response determined by the timescale for thermal diffusion.

4. Numerical simulations of transient 1

A full series of numerical simulations in which we reproduce and extend the laboratory results is beyond the scope of this study. To accurately resolve local variations in the temperature and viscosity structure of the hot thermal boundary layer, and the corresponding heat fluxes, for a larger range of Ra–Pe–λ_t–A conditions during the early part of transient 1 is particularly difficult. However, we can use numerical simulations to explore the robustness of a number of qualitative features of the mixed mode regime. Here we carry out a small suite of calculations in which we apply no-slip or free-slip basal boundary conditions with wrap-around sidewalls in a 4×1 modeling domain. This will allow us to explore the degree to which the rigid boundary conditions used in our lab experiments affect our main results regarding lower boundary layer dynamics. For applications to Venus it is useful also to consider whether volumetric internal heating will reduce the temperature difference between the hot boundary and interior mantle enough to alter or inhibit the mixed mode of convection observed in the experiments. Although a complete analysis of the effects of various ratios of internal to basal heating is beyond the scope of this paper we present the results of two cases (60% and 97% internal heating) to place bounds on possible behavior.

Some specific differences to the basic setup of our experiments require discussion. In the presence of a

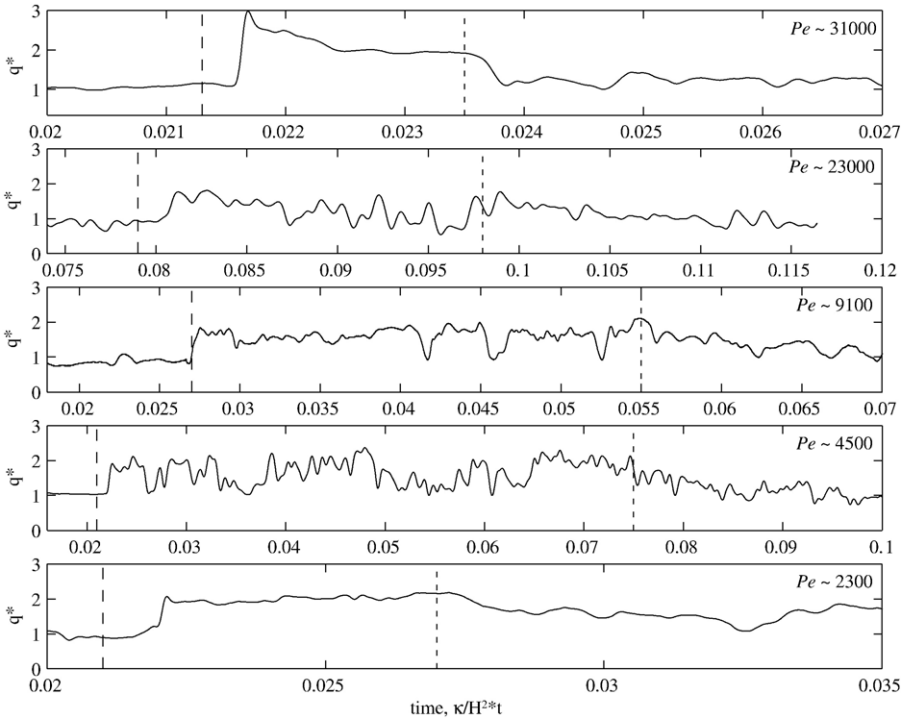

Fig. 9. Time series of local heat flux for all of the experiments in Table 2. The onset and cessation of the forced flow is indicated with dashed lines as before.

free-slip basal boundary condition a squeeze layer will not form as it did in our experiments. We thus investigate whether low viscosity plumes will form during the transient by conductive heat transfer from the hot boundary alone. One effect of employing wrap-around sidewall boundary conditions is to reduce the effects of rigid sidewalls on the structure and heat transfer properties of the cold downwellings. In our experiments extensive viscous coupling of the descending cold material to the sidewalls probably reduced the amount of cooling carried to the floor because the coldest and most viscous material may have remained adhered to the walls.

4.1. Method

We use the CITCOM finite element code to solve the equations of convection in the limit of infinite Prandtl Number [63]. Numerical simulations are initially run to statistically steady-state conditions and the accuracy of the code is tested against standard benchmark solutions [64]. For these runs, convergence testing is also performed to assure that simulations are well resolved. Simulations reported are performed using 64×64 meshes over any 1×1 patch.

The non-dimensional system of equations with the Boussinesq approximation is:

$$\partial_i u_i = 0 \tag{4}$$

$$\partial_j[2\mu\varepsilon_{ij}] = \partial_i p + Ra_h T\,\hat{k} \tag{5}$$

$$\partial_t T + \mu_i \partial_i T = \partial_i^2 T \tag{6}$$

$$\rho = [1-\alpha(T-T_0)], \tag{7}$$

where Rayleigh numbers $Ra_h = 10^6$–10^8 (for steady-state runs) and $Ra_h = 10^8$ (for transient runs) are based on a viscosity at the hot boundary temperature and physical properties defined in the usual way [42]. Here, u_i is the velocity vector, μ is the viscosity, T is temperature, ε_{ij} is the strain rate tensor, p is pressure, $\hat{k}$ is the vertical unit vector, and ρ is the density. Subscripts of zero indicate reference values. Eqs. (4)–(6) are the continuity, momentum and energy equations for incompressible flow. Eq. (7) is the linearized equation of state.

We performed two sets of simulations. The first set is used to explore lower boundary layer structure in the end-member situations of stagnant and active-lid convection at statistically steady state. The second set of simulations explores the transient situation in which

the stagnant-lid transitions to an active-lid mode of convection.

For the first set of simulations, we apply a viscoplastic mantle rheology that can allow for an active-lid mode of convection and for an internal mantle viscosity that depends strongly on temperature [53]. That is, for convective stresses below a critical yield stress, τ_{yield}, the viscosity is $\mu = A\exp(-\gamma T)$, which is similar to corn syrup (Table 1) and consistent with a mantle deforming in the diffusion creep limit. Here, the rheological temperature scale $\gamma = -d/dt(\ln(\mu))$ [56]. For all simulations reported on, the non-dimensional activation temperature is set to 13.815511. This leads to a six order of magnitude viscosity variation across the modeling domain. For stresses above τ_{yield}, however, the rheology is nonlinear and the effective viscosity is $\mu = \tau_{yield}/I$, where I is the second strain-rate invariant. A useful consequence of this shear-thinning rheology is that where convective stresses exceed τ_{yield} the effective viscosity become very small such that strain is localized in narrow shear zones and the stagnant-lid fails in shear and founders, resulting in active-lid convection. The second set of simulations is designed to follow the lab experiments more closely and the viscosity depends only on temperature. That is, no yield stress is employed. Rather, as with the laboratory experiments, the stagnant lid is forced to become active by imposing velocity boundary conditions at the surface of the modeling domain.

4.2. Results

Snapshots of stagnant-lid and active-lid regimes under statistically steady-state conditions are shown in Fig. 10. As with our experiments, the subduction and stirring of the cold thermal boundary layer (blue) leads, in turn, to a lower internal mantle temperature, a greater temperature drop across the hot thermal boundary layer (red), and a larger hot thermal boundary layer viscosity ratio than the stagnant-lid case. In the stagnant-lid case $\lambda_h = 4$, quantitatively identical to our experiments, and the (two-dimensional) upwelling structures are analogous to thermals. In contrast, in the active-lid case $\lambda_h = 10^3$, corresponding to an internal temperature that is the mean of the two boundaries, and upwellings are analogous to the low viscosity plumes observed in our experiments and elsewhere [31]. When internal heating is included in the calculations the internal temperature is proportionally higher in both regimes and λ_h smaller.

Examples from a series of calculations exploring the transient regime are shown in Fig. 11. For these calculations a horizontal surface velocity boundary condition is applied to a stagnant-lid starting model to force a stagnant to active-lid transition. The surface velocity is symmetrical about the center of the modeling domain and the non-dimensional values of the horizontal velocity are +600 to the left of the domain center and −600 to the right of center. These values are below the statistically steady state surface velocity that resulted from active-lid simulations using a viscoplastic rheology (Fig. 10). This allowed us to confirm that for the transient cases the imposed surface velocity condition was not doing external work on the system beyond that which would result from internal buoyancy forces alone. In principal, transient cases could be explored using viscoplastic models with no imposed surface velocity. However, preliminary simulations showed

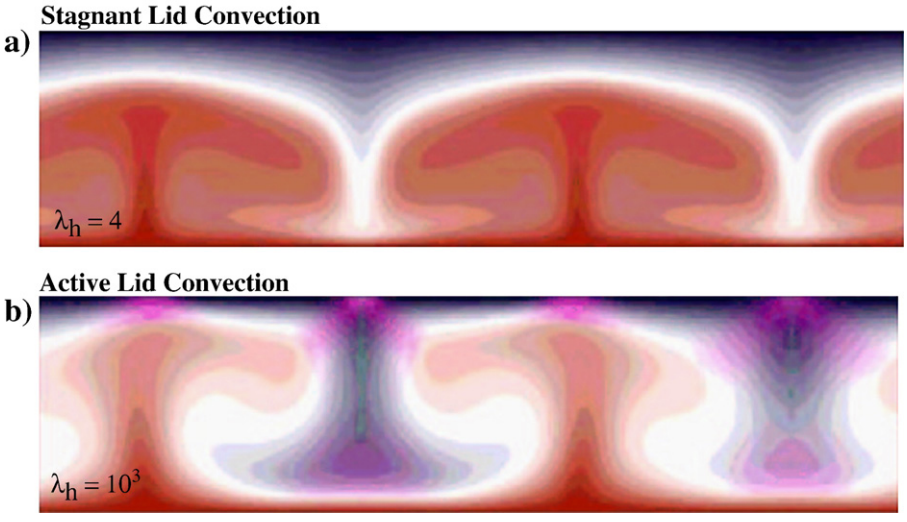

Fig. 10. Snapshots of a) stagnant-lid and b) active-lid convection under statistically steady-state conditions. $Ra = 10^6$. See text for discussion.

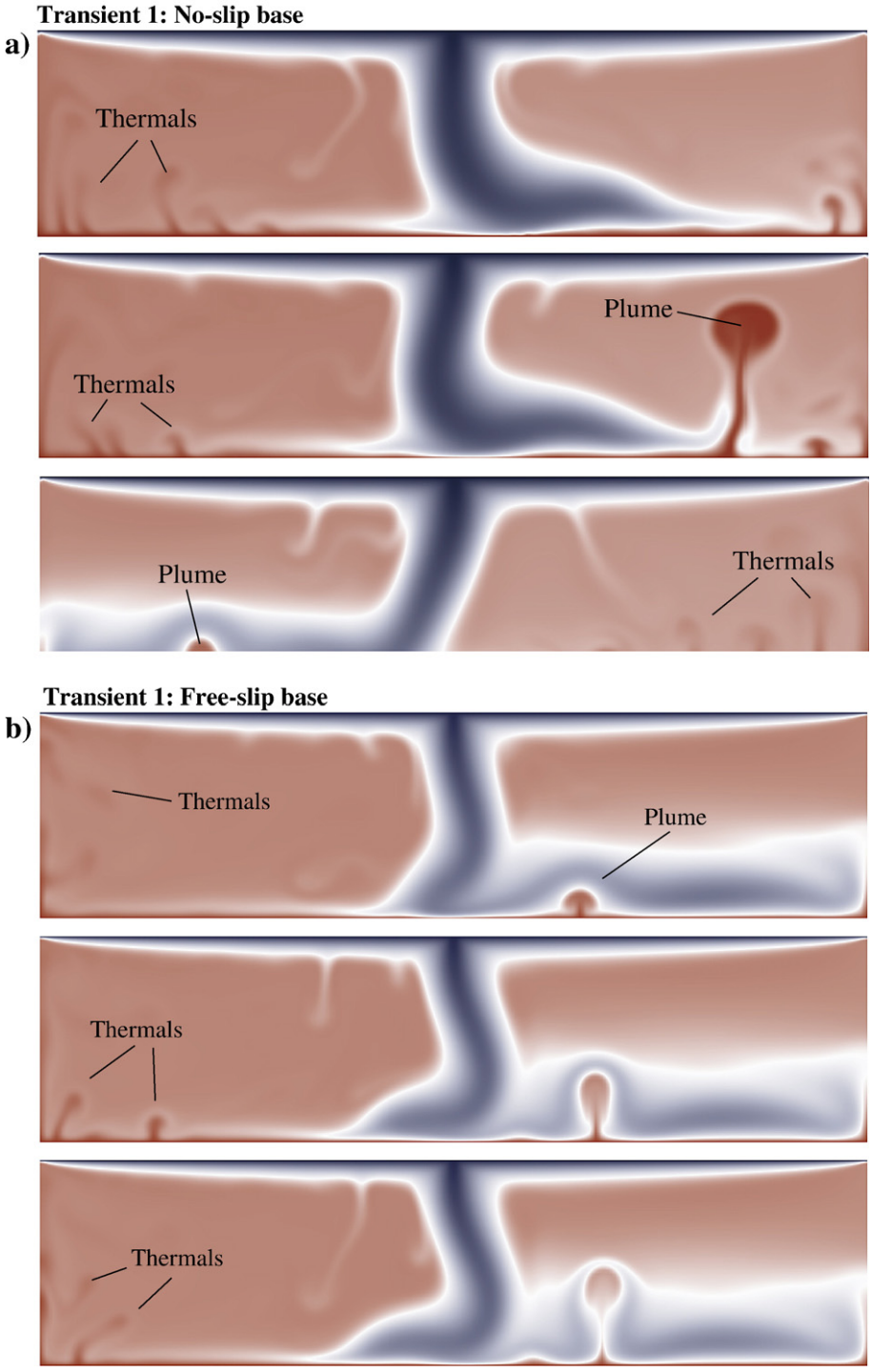

Fig. 11. Snapshots from several series of calculations of transient 1 (following the stagnant-lid regime indicated in Fig. 10a) in the presence of a) free-slip, b) no-slip basal boundaries, c) 60% internal heating, and d) 97% internal heating. $Ra = 10^8$. Sidewall boundary conditions are wrap-around. Except in the unrealistic case of 97% internal heating, approximately isoviscous thermals form in the hot boundary layer ahead of the advancing cold front, whereas low viscosity plumes, carrying a larger excess temperature, form behind.

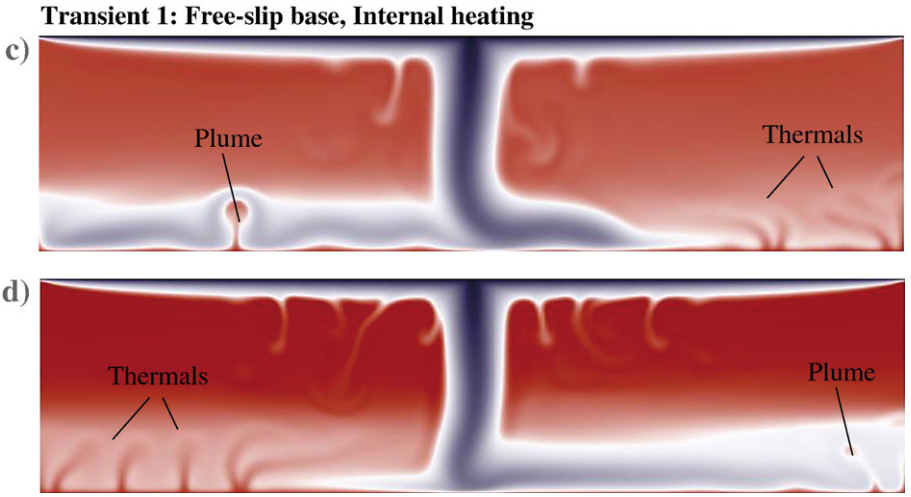

Fig. 11 (*continued*).

added complexities in that the aspect ratio of convection cells could rapidly change during the transient state, which effected lower boundary layer dynamics. Further, depending on the choice of yield stress, episodic regimes could result in which the upper boundary layer became active for short time bursts and then returned to a stagnant-lid state. Our intent, at this first stage of work, is to isolate the effects of subduction and stirring of the cold boundary layer on lower boundary layer dynamics independent of such added complexities. Thus, we opt for an approach more in line with the laboratory experiments. This approach allows the aspect ratio of cells to remain fixed through the transitional regime. We are aware that aspect ratio changes deserve future investigations but this would go beyond the scope of this paper.

A no-slip basal boundary condition is applied in Fig. 11a. As in our experiments, the subduction and spreading of the cold thermal boundary layer along the hot boundary traps a squeeze layer and causes a monotonic increase in hot thermal boundary layer thickness down stream. Large lateral variations in the vertical temperature difference across the thermal boundary layer drive a similar mixed mode of convection. Whereas thermals, carrying a small excess temperature, are observed downstream of the cold front, low viscosity plumes, carrying a much higher excess temperature, rise through the cold layer. The timescales and positions of such plume instabilities are influenced by the rate at which cold material spreads. In Fig. 11b we apply a free-slip basal boundary condition and also obtain a mixed mode flow regime with some subtle differences. In the absence of viscous coupling to the bottom boundary the thermal boundary grows at the base of the cold current by vertical thermal conduction alone, and is consequently more uniformly thick (except near the downwelling). The timing and location of plume-forming instabilities is influenced less by the lateral advection of cold material.

In Fig. 11c and d we show results from two calculations including volumetric internal heating. The initial state for both calculations is a stagnant-lid regime under statistically steady-state conditions. In Fig. 11c, the ratio of internal to basal heating is 60/40 and we find that following the initiation of an active-lid regime a mixed mode of convection again emerges with plumes rising through the cold layer and thermals rising ahead of the advancing front of cold material. One difference to the purely basally heated cases is that a smaller fraction of the rising thermals ascends to the top of the mantle [cf. [65]]. In Fig. 11d the extreme case of nearly purely internally heated convection (97%) is shown. A mixed mode of convection is apparent near the hot boundary. However, the temperature difference between hot upwellings and surrounding mantle is sufficiently small that neither plumes nor thermals rise across the full depth of the mantle before diffusing away.

5. Conclusions

Following the initiation of subduction, the spatial and temporal dynamics of the hot thermal boundary layer depend on local conditions that vary in time. Results from our experiments and numerical simulations show that spreading of the cold stagnant lid along the hot boundary leads to a mixed mode of convection with

approximately isoviscous thermals forming ahead of the cold front and low viscosity plumes forming behind. This regime will persist for the time required for the cold material to cover the hot boundary. For a given system aspect ratio the longevity of the mixed mode regime decreases with increasing *Pe* because the timescale to cover the hot boundary with cold material is reduced. The magnitude of the local temperature and viscosity variations giving rise to low viscosity plumes increase with *Pe*. These variations correspond also with variations in heat flux. One interesting result is that the local heat flux can exceed the steady-state active-lid value during transient 1.

Comparison with our numerical simulations suggests that this regime will also emerge in the presence of intermediate extents of internal heating, and for no- and free-slip basal boundaries. However, the relative timing and spatial relationship between thermals and low viscosity plumes probably depends quantitatively on the mechanical coupling to the hot boundary (e.g. Fig. 10) and may depend on the relative proportions of internal to basal heating. In particular, thermal formation observed directly ahead of the advancing cold front (Fig. 4) may be enhanced even further by the lateral advection, or 'bulldozing', of boundary layer fluid if the basal boundary condition is free-slip. In addition, the timescale for plume-forming instabilities upstream from the cold front may be reduced if a significant squeeze layer is trapped during spreading, a feature which is enhanced for rigid boundaries. The spacing of plumes and thermals will depend on both the mechanical coupling to the hot boundary and on variations in the vertical and lateral viscosity structure of the hot thermal boundary layer (e.g. [61]).

6. Applications to Venus

6.1. The coexistence and relative timing of Atla and Beta Regio and BAT coronae

Our combined experimental and numerical results show that the contemporaneous coexistence of uncompensated BAT coronae and the Atla and Beta highland regions can indeed be explained as a result of a "mixed-mode" style of mantle convection from the core–mantle boundary (i.e. Fig. 1b). Such a regime can arise during a thermal transient following a large-scale lithospheric overturn. It is expected to persist for a timescale that depends on the spatial extent and geometry of the overturn, as well as the rates and styles of subduction and subsequent mantle stirring. That this regime is observed for no- and free-slip basal boundary conditions suggests also that it will emerge if Venus has a liquid or a solid core [66,67]. Significantly, this style of upwelling flow is not consistent with ours and previous laboratory experiments and numerical studies on stagnant-lid and active-lid convection under thermally steady-state conditions. Thus, whereas we confirm the plausibility of the model proposed by Johnson and Richards [5] (Fig. 1), we also identify the highly restrictive conditions in which such a regime may occur.

A constraint on the relative timing of uncompensated BAT coronae and the Atla and Beta highlands may be drawn from our work. Johnson and Richards [5] suggest on thermal grounds that the population of BAT coronae due to mantle thermals are younger than the isostatically compensated coronae distributed broadly over the surface of Venus. That is, assuming all coronae are initially a surface expression of mantle thermals, one way to distinguish the two populations of coronae is to explain the current positive gravity anomalies associated with BAT corona in terms of thermal buoyancy sources in the mantle that decay over time. Thus, the compensated coronae have equilibrated thermally by thermal diffusion and perhaps melt production [68]. A second characteristic that defines the two populations is the geometric concentration of uncompensated coronae within the BAT region. Johnson and Richards [5] suggest that the focussing of these features within BAT is due to a combination of effects related to the spreading of cold sublithospheric drips at the core–mantle boundary and upwelling flows into Atla and Beta (Fig. 1b). Alternatively, as investigated here, the clustering of thermals as well as the formation of low viscosity axisymmetric upwellings giving rise to Atla and Beta, may be governed by the spreading of an overturned layer of cold lithosphere at the core–mantle boundary: clustered thermals form ahead of the advancing front of cold lithosphere as it 'bulldozes' and thickens the hot TBL ahead of it, and low-viscosity plumes form behind. Indeed, the concentration of dynamically supported coronae within BAT is not inconsistent with thermals being focused by an axisymmetric mantle return flow occurring in response to a lithospheric overturn in a spherical geometry [69]. The relative timing of the surface expressions of both upwelling features then depends on the timescales for their formation and rise through the Venusian mantle.

Quantitative constraints on the timescales for the formation of both types of upwelling features at the hot boundary are complicated by interactions between the spreading cold fluid, the hot thermal boundary layer and the hot boundary itself. Figs. 4 and 6 suggest that thermal formation is enhanced directly ahead of the advancing front due to advective thickening of the thermal boundary

layer. Consequently the period of thermal formation is less than that which would occur downstream of the cold front by thermal diffusion alone. However, the magnitude of the effect depends on *Pe*, which is not constrained for Venus, and on the mechanical coupling to the core–mantle boundary. The timescale of plume formation depends on the initial thickness of the trapped squeeze layer (no-slip boundaries) as well as the rates of vertical thermal diffusion and lateral advection (no-and free-slip boundaries).

Whereas constraints on the timescale of formation are not straightforward, estimates of the relative times for plumes and thermals to rise across the mantle can be obtained readily. Such estimates thus indicate a lower bound on the relative ages of uncompensated BAT coronae and the Atla and Beta regions. We note that both thermals and plumes are observed to form closely in time in all experiments and simulations. We assume that mantle deformation is in the diffusion creep limit and take the viscosity $\mu=\mu_o\exp(-\gamma T)$, where μ_0 is a reference viscosity and γ is again the rheological temperature scale. Low viscosity plume heads are expected to rise faster than thermals because they are both larger and carry a greater excess temperature. The ratio of the timescale of a thermal to ascend across the mantle to that for a nascent plume head (i.e. starting plume) is $\tau_{th}/\tau_{pl}\sim(\Delta T_{pl}/\Delta T_{th})(d_{pl}/d_{th})^2\sim(\Delta T_{pl}/\Delta T_{th})(\lambda_h^{pl}/\lambda_h^{th})^{2/3}$, where the diameters of plumes, d_{pl}, and thermals, d_{th}, are expected to scale with the respective critical thermal boundary layer thickness such that $d_{pl}/d_{th}\sim(\lambda_h^{pl}/\lambda_h^{th})^{1/3}$ (e.g. [61]). We take $\gamma=0.0145$, which gives $\lambda_h^{th}\approx 4$ (the stagnant-lid value) for a thermal excess temperature $\Delta T_{th}\approx 100$ °C as well as $\lambda_h^{pl}\approx 100$ and $\lambda_h^{pl}\approx 200$ for plume excess temperatures of $\Delta T_{pl}\approx 200$ °C and $\Delta T_{pl}\approx 300$ °C, consistent with parameters inferred for low viscosity mantle plumes in the Earth (e.g. [31]). Assuming that the mean diameter of isostatically compensated coronae indicate the average diameter of underlying mantle thermals we take $d_{th}\approx 200$ km. Applying these values we obtain $d_{pl}/d_{th}\approx 1.6$–2.7 and $\tau_{th}/\tau_{pl}\approx 5$–$20$. In addition, for $200\le\Delta T_{pl}\le 300$ °C, an average Venusian mantle viscosity of 5×10^{20} Pa s and reasonable physical properties [26,54,55] the timescale for a low viscosity plume to rise across the full depth of the mantle is expected to be 60–20 Myr, respectively [70,71]. In contrast, nearly isoviscous thermals are expected to take around 300 Myr to traverse the Venusian mantle.

If the plumes and thermals forming in response to a lithospheric overturn emerge from the core–mantle boundary region closely in time, it is reasonable to expect the Atla and Beta highland regions to precede BAT coronae by >250 Myr. With additional information about the uplift history of the Atla and Beta highlands, this relative timing also constrains the absolute age of BAT coronae. In a recent paper, Vezolainen et al. [27] apply an elegant combination of results from geological, geomorphological and cratering studies to argue that the timescale for the uplift of Beta Regio is less than about one-half the mean surface age. Assuming a mean surface age of 700–800 Myr, this result implies that the uplift of Beta occurred over the last 350–400 Myr, which is comparable to the timescale for a thermal to rise across the mantle. Thus, it is reasonable to suggest that some fraction of the uncompensated BAT coronae may have formed within the last 100 Myr. Hence, we propose the following rough timeline of events: i) Venus experiences a gravitational collapse of the stagnant-lid (700 Ma); ii) pieces of the cold lid reach and spread across the CMB, forming squeeze layers beneath them and 'bulldozing' the hot TBL ahead of them (500 Ma); iii) low viscosity plumes from the squeeze layer reach the surface and form Atla and Beta Regio (350 Ma); and iv) thermals formed in the bulldozed TBL between the advancing cold fronts responsible for the Atla and Beta plumes finally reach the surface, concentrated in the BAT region (<100 Ma).

6.2. Link between coronae and mantle thermals: implications for mantle structure

If dynamically supported BAT coronae are created by thermals ascending from the core–mantle boundary region of Venus, they are a useful probe of the internal structure and phase relations in the mantle. Indeed, whether a rising thermal carrying a relatively small temperature excess can rise through the full depth of a mantle that may be characterized by an Earth-like endothermic post-spinel phase transition at 740 km depth [72,73], is not *a priori* obvious. Thus, that thermals cross the mantle and produce coronae with the observed size distribution, provides, in principle, a constraint on the nature of the Venusian interior. However, similarity between the interior phase relations of Earth and Venus must be treated with caution because of potentially significant differences between the background mantle temperatures of these planets. In particular, at 740 km depth the endothermic γ-spinel to perovskite + magnesiowustite transition will cross the exothermic majorite to perovskite transition boundary if the temperature is 200–300 °C greater than in the Earth and the ascent of thermals will be enhanced rather than inhibited [74].

Any estimate of the time-averaged interior temperature of Venus depends on the predominant mode(s) of mantle convection, which remains a matter for debate. Whereas

an active-lid or episodic mode of mantle convection implies a mantle temperature comparable to the Earth, a stagnant-lid mode suggests temperatures a few hundred degrees hotter [42,53] and implies that thermals will be at a temperature above the majorite–perovskite–magnesiowustite triple point and unimpeded by a 740 km phase boundary [74]. It is thus instructive to consider the alternative end-member case of an interior temperature comparable to Earth in which the temperature of mantle thermals remains below the majorite–perovskite–magnesiowustite triple point at 740 km depth. For a given excess temperature, ΔT_{ex}, the magnitude of which depends on both the mantle viscosity law and a rate of volumetric internal heating [41], a number of studies have shown that the penetration of thermals will depend on the Clapeyron slope, Γ, density change, $\Delta\rho_{\mathrm{ph}}$, and characteristic temperature change, L/C_{p}, associated with a given phase transition, as well as the stabilizing density difference related to mantle chemical layering, $\Delta\rho_c$ [75–80]. Here, L is the latent heat absorbed (endothermic) or released (exothermic) as a result of the phase change and C_p is the specific heat at constant pressure. Following Christensen and Yuen [76] and Nakakuki et al. [78] the penetration of mantle thermals across the 740 km phase boundary is governed by two dimensionless parameters. The phase change buoyancy number, $P=(\Gamma\Delta\rho_{ph}/\rho^2\alpha gH)$, which expresses a balance between the stabilizing buoyancy stress acting against the upward deflection of a phase boundary with a negative Clapeyron slope and the (global) buoyancy stress driving basally-heated mantle convection, must be larger than $P_{crit}=-0.4$ to -0.2. For an endothermic phase change the excess temperature following the phase change, $\mathbf{T}=1-(L/C_p\Delta T_{ex})>0$.

For reasonable physical properties ($\alpha=2.5\times10^{-5}\mathrm{C}^{-1}$, $\Delta\rho_{ph}=300$ kg m^{-3}) and a background temperature at 740 km of 1600 °C, the phase change number $P>P_{crit}$ if $\Gamma>-2$ to -4 MPa/°C, which is consistent with published values (e.g. [81]). This suggests that it is reasonable to expect thermals to pass through such a transition much the same way plumes penetrate the 670 km phase transition on Earth [82]. However, inclusion of the effect of latent heat makes this conclusion potentially less convincing. The latent heat absorbed by the phase change is 50–70 kJ/kg (e.g. [83]). Taking $C_{\mathrm{p}}\approx1$ kJ kg^{-1} °C^{-1} and a nominal $\Delta T_{\mathrm{ex}}=100$ °C, consistent with $\lambda_{\mathrm{h}}\approx1$ (a lower bound that may occur in the presence of internal heating), the minimum remaining excess temperature $0.3\le T\le0.5$, implying that although possible, rising thermals may lose up to 50–70% of their buoyancy as they pass through this phase transition.

To the extent that the physical state of the Venusian mantle is similar to the Earth it is reasonable to conclude that an endothermic phase transition at 740 km may strongly inhibit the passage of rising thermals. The chances for survival are enhanced if thermals merge as they rise (e.g. [65]) but this is not supported by surface observations: The distribution of coronae diameters has a well-defined mean of around 200 km with only a small number of much larger features. Taken together with the discussion above, this result supports a speculation that a link between mantle thermals and coronae requires the Venusian mantle to be considerably hotter than the Earth's.

6.3. Future directions

Our results suggest a number of directions for future study. Analyses of the spatial and temporal relationships between thermals and low viscosity plumes for a range of Pe–Ra–λ_{t} conditions in Cartesian and spherical systems will be useful for understanding the geometric distribution and timing of resulting coronae and plume-related highlands. Indeed, the geometric relationship between the BAT coronae and the BAT highlands themselves may provide constraints on the scale and geometry of a lithospheric overturn on Venus. An additional interesting result is that during a transient following an overturn the local core heat flux can exceed the steady-state active-lid value. Depending on the spatial distribution and magnitude of such heat flux maxima, such a condition raises the possibility of a short-lived core dynamo.

Acknowledgements

We thank Dave Stegman for his thought-provoking review. We also thank ADM for donating corn syrup to our lab. This research has been supported by the Natural Sciences and Engineering Research Council of Canada, the Canadian Institute for Advanced Research, and by NSF grant EAR-0448871 to A. L.

References

[1] E.R. Stofan, V.L. Sharpton, G. Schubert, G. Baer, D.L. Bindschadler, D.M. Janes, S.W. Squyres, Global distribution and characteristics of coronae and related features on Venus: implications for origin and relation to mantle processes, JGR 97 (1992) 13347–13378.

[2] E.R. Stofan, S.E. Smrekar, S.W. Tapper, J.E. Guest, P.M. Grindrod, Preliminary analysis of an expanded corona database for Venus, GRL 28 (2001) 4267–4270.

[3] L.S. Glaze, E.R. Stofan, S.E. Smrekar, S.M. Bologa, Insights into corona formation through statistical analyses, J. Geophys. Res. 107 (2002), doi:10.1029/2002JE001904.

[4] V.L. Hansen, J.J. Willis, W.B. Banerdt, Tectonic Overview and Synthesis, in: S.W. Bougher (Ed.), Venus II, Univ. of Ariz. Press, Tucson, 1997, pp. 797–844.

[5] C.L. Johnson, M.A. Richards, A conceptual model for the relationship between coronae and large-scale mantle dynamics on Venus, J. Geophys. Res. 108 (2003).
[6] D.M. Janes, S.W. Squyres, D.L. Bindschadler, G. Baer, G. Schubert, V.L. Sharpton, E.R. Stofan, Geophysical models for the formation and evolution of coronae on Venus, JGR 121 (1992) 16055–16067.
[7] S. Smrekar, E.R. Stofan, Coupled upwelling and delamination: a new mechanism for coronae formation and heat loss on Venus, Science 277 (1997) 1289–1294.
[8] E.R. Stofan, A.W. Brian, J.E. Guest, Resurfacing styles and rates on Venus: assessment of 18 Venusian quadrangles, Icarus 173 (2005) 312–321.
[9] R.R. Herrick, R.J. Phillips, Geological correlations with interior density structure on Venus, J. Geophys. Res. 97 (1992) 16017–16034.
[10] G. Schubert, D. Bercovici, P.J. Thomas, D.B. Campbell, Venus coronae - Formation by mantle plumes, Abstracts Submitted to the 20th Lunar and Planetary Science Conference, 1989, pp. 968–969.
[11] D.M. Jurdy, M. Stefanick, Correlation of Venus surface features and geoid, Icarus 139 (1999) 93–99.
[12] V.L. Hansen, Venus diapirs: thermal or compositional? GSA Bull. 115 (2003) 1040–1052.
[13] D.M. Janes, S.W. Squyres, Viscoelastic relaxation of topographic highs on Venus to produce coronae, J. Geophys. Res. 100 (1995) 21,173–21,187.
[14] D.M. Koch, M. Manga, Neutrally buoyant diapirs: a model for Venus coronae, Geophys. Res. Lett. 23 (1996) 225–228.
[15] T. Hoogenboom, G.A. Houseman, Rayleigh–Taylor Instability as a mechanism for coronae formation on Venus, Icarus (in review), 2005.
[16] A.J. Dombard, Coronae on Venus as products of magmatic loading of the crust over transient plume heads: consequences for surface deformation and volcanism, abstract, AGU Chapman Conference on Exploring Venus as a Terrestrial Planet, 2006, p. 19.
[17] D.T. Sandwell, G. Schubert, Flexural ridges, trenches and outer rises around coronae on Venus, J. Geophys. Res. 97 (1992) 16069–16083.
[18] J.E. DeLaughter, D.M. Jurdy, Corona classification by evolutionary stage, Icarus 139 (1991) 81–92.
[19] M. Simons, S.C. Solomon, B.H. Hager, Localization of gravity and topography: constraints on the tectonics and mantle dynamics of Venus, Geophys. J. Int. 131 (1997) 24–44.
[20] N. Schaeffer, M. Manga, Interaction of rising and sinking mantle plumes, Geophys. Res. Lett. 28 (2001) 455–458.
[21] A.M. Jellinek, A. Lenardic, M. Manga, The influence of interior mantle temperature on the structure of plumes: heads for Venus, tails for Earth, Geophys. Res. Lett. 29 (2002), doi:10.1029/2001GL014624.
[22] A.M. Jellinek, H.M. Gonnerman, M.A. Richards, Plume capture by divergent plate motions: implications for the distribution of hotspots, geochemistry of mid-ocean ridge basalts, and estimates of the heat flux at the core–mantle boundary, Earth Planet. Sci. Lett. 205 (2003) 361–378.
[23] J.A. Whitehead Jr., D.S. Luther, Dynamics of laboratory diapir and plume models, JGR 80 (1975) 705–717.
[24] D.E. Loper, F.D. Stacey, The dynamical and thermal structure of deep mantle plumes, Phys. Earth Planet. Inter. 33 (1983) 304–317.
[25] M.A. Richards, R.A. Duncan, V.E. Courtillot, Flood basalts and hot-spot tracks: plume heads and tails, Science 246 (1989) 103–107.
[26] F. Nimmo, D. McKenzie, Modeling plume-related uplift, gravity and melting on Venus, Earth Planet. Sci. Lett. 145 (1996) 109–123.
[27] A.V. Vezolainen, V.S. Solomatov, J.W. Head, A.T. Basilevsky, L.-N. Moresi, Timing of formation of Beta Regio and its geodynamical implications, J. Geophys. Res. 108 (E1) (2003), doi:10.1029/2002JE001889.
[28] J.S. Turner, Buoyancy Effects in Fluids, Cambridge Univ. Press, Cambridge, 1973, 368 pp.
[29] M. Ogawa, G. Schubert, A. Zebib, Numerical simulation of three-dimensional thermal convection in a fluid with strongly temperature-dependent viscosity, J. Fluid Mech. 233 (1991) 299–328.
[30] M. Manga, D. Weeraratne, Experimental study of non-Boussinesq Rayleigh–Benard convection at high Rayleigh and Prandtl numbers, Phys. Fluids 11 (1999) 2969–2976.
[31] A.M. Jellinek, M. Manga, Links between long-lived hotspots, mantle plumes, D″ and plate tectonics, Rev. Geophys. 42 (3) (2004) RG3002, doi:10.1029/2003RG000144.
[32] S. Morris, D. Canright, A boundary layer analysis of Benard convection in a fluid of strongly temperature-dependent viscosity, Phys. Earth Planet. Inter. 36 (1984) 355–373.
[33] R.W. Griffiths, I.H. Campbell, On the dynamics of long-lived plume conduits in the convecting mantle, Earth Planet. Sci. Lett. 103 (1991) 214–227.
[34] A. Lenardic, W.M. Kaula, Tectonic plates, D″ thermal structure, and the nature of mantle plumes, J. Geophys. Res. 99 (1994) 15697–15708.
[35] A.M. Jellinek, H.M. Gonnerman, M.A. Richards, Plume capture by divergent plate motions: implications for the distribution of hotspots, geochemistry of mid-ocean ridge basalts, and estimates of the heat flux at the core–mantle boundary, Earth Planet. Sci. Lett. 205 (2003) 361–378.
[36] R.C. Kerr, C. Mèriaux, Structure and dynamics of sheared mantle plumes, Geochem. Geophys. Geosyst. 5 (2004) Q12009, doi:10.1029/2004GC000749.
[37] P. Olson, H. Singer, Creeping plumes, J. Fluid Mech. 158 (1985) 511–531.
[38] M. Manga, D. Weeraratne, S.J.S. Morris, Boundary-layer thickness and instabilities in Benard convection of a liquid with a temperature-dependent viscosity, Phys. Fluids 13 (2001) 802–805.
[39] U. Hansen, A. Ebel, Time-dependent thermal convection — a possible explanation for a multiscale flow in the Earth's mantle, Geophys. J. 94 (1988) 181–191.
[40] H.-C. Nataf, Mantle convection, plates and hotspots, Tectonophysics 187 (1991) 355–373.
[41] V.S. Solomatov, L.-N. Moresi, Scaling of time-dependent stagnant lid convection: application to small-scale convection on the Earth and other terrestrial planets, J. Geophys. Res. 105 (2000) 21795–21818.
[42] G. Schubert, D.L. Turcotte, P. Olson, Mantle Convection in the Earth and Planets, Cambridge Univ. Press, Cambridge, 2001, 940 pp.
[43] V. Thayalan, A.M. Jellinek, A. Lenardic, Recycling the lid: Effects of subduction and stirring on the boundary layer dynamics in bottom-heated planetary mantle convection, Geophys. Res. Lett. 33 (2006) L20318, doi:10.1029/2006GL027668.
[44] R.J. Phillips, R.F. Raubertas, R.E. Arvidson, I.C. Sarkar, R.R. Herrick, N. Izenberg, R.E. Grimm, Impact craters and Venus resurfacing history, J. Geophys. Res. 97 (E10) (1992) 15923–15948.
[45] R.G. Strom, G.G. Schaber, D.D. Dawson, The global resurfacing of Venus, J. Geophys. Res. 99 (E5) (1994) 10899–10926.

[46] W.B. McKinnon, K.J. Zahnle, B.A. Ivanov, H.J. Melosh, Cratering on Venus: Models and observations, in: S.W. Bougher (Ed.), Venus II, Univ. of Ariz. Press, Tucson, 1997, pp. 969–1014.
[47] S.A. Hauck, R.J. Phillips, M.H. Price, Venus: crater distribution and plains resurfacing models, J. Geophys. Res. 103 (1998) 13635–13642.
[48] J.E. Guest, E.R. Stofan, A new view of the stratigraphic history of Venus, Icarus 139 (1999) 55–66.
[49] E.M. Parmentier, P.C. Hess, Chemical differentiation of a convecting planetary interior: consequences for a one plate planet such as Venus, Geophys. Res. Lett. 19 (1992) 2015–2018.
[50] G.G. Schaber, R.G. Strom, H.J. Moore, L.A. Soderblom, R.L. Kirk, D.U. Chadwick, D.D. Dawson, L.R. Gaddis, J.M. Boyce, J. Russell, Geology and distribution of impact craters on Venus: what are they telling us? J. Geophys. Res. 97 (E8) (1992) 13257–13301.
[51] D.L. Turcotte, An episodic hypothesis for Venusian tectonics, JGR 98 (17) (1993) 061–068.
[52] D.L. Turcotte, G. Morein, D. Roberts, B.D. Malamud, Catastrophic resurfacing and episodic subduction on Venus, Icarus 139 (1999) 49–54.
[53] L.-N. Moresi, V. Solomatov, Mantle convection with a brittle lithosphere: thoughts on the global tectonic style of the Earth and Venus, Geophys. J. Int. 133 (1998) 669–682.
[54] V.S. Solomatov, L.-N. Moresi, Stagnant lid convection on Venus, J.Geophys. Res. 101 (1996) 4737–4753.
[55] F. Nimmo, D. McKenzie, Volcanism and tectonics on Venus, Annu. Rev. Earth Planet. Sci. 26 (1998) 23–51.
[56] A.M. Jellinek, H.M. Gonnerman, M.A. Richards, Plume capture by divergent plate motions: implications for the distribution of hotspots, geochemistry of mid-ocean ridge basalts, and estimes of the heat flux of the core-mantle boundary, Earth Planet. Sci. Lett. 205 (2003) 361–378.
[57] E. Tan, M. Gurnis, L. Han, Slabs in the lower mantle and their modulation of plume formation, G3 3 (11) (2002) 1067, doi:10.1023/2001GC000238.
[58] D. Snyder, S. Tait, A flow-front instability in viscous gravity currents, J. Fluid Mech. 369 (1998) 1–21.
[59] Selig, A theoretical prediction of salt dome patterns, Geophysics 30 (1965) 633–643.
[60] M.A. Biot, H. Odé, Theory of gravity instability with variable overburden and compaction, Geophysics 30 (1965) 213–227.
[61] J.R. Lister, R.C. Kerr, The effect of geometry on the gravitational-instability of a buoyant region of viscous-fluid, J. Fluid Mech. 202 (1989) 577–594.
[62] H.M. Gonnerman, A.M. Jellinek, M.A. Richards, M. Manga, Modulation of mantle plumes and heat flow at the core mantle boundary by plate-scale flow: results from laboratory experiments, Earth Planet. Sci. Lett. 234 (2005) 317–333.
[63] L.-N. Moresi, V.S. Solomatov, Numerical investigation of 2D convection with extremely large viscosity variations, Phys. Fluids 7 (1995) 2154–2162.
[64] A. Blackenbach, F. Busse, U. Christensen, L. Cserepes, D. Gunkel, U. Hansen, H. Harder, G. Jarvis, M. Koch, G. Marquart, D. Moore, P. Olson, H. Schmeling, T. Schnaubelt, A benchmark comparison for mantle convection codes, Geophys. J. Int. 98 (1989) 23–38.
[65] S. Labrosse, Hotspots, mantle plumes and core heat loss, Earth Planet. Sci. Lett. 199 (2002) 147–156.
[66] F. Nimmo, Why does Venus lack a magnetic field? Geology 30 (2002) 987–990.
[67] A.S. Konopliv, C.F. Yoder, Venusian k2 tidal Love number from Magellan and PVO tracking data, Geophys. Res. Lett. 23 (1996) 1857–1860.
[68] A.J. Dombard, C.L. Johnson, M.A. Richards, S.C. Solomon, A transient plume melting model for coronae on Venus, abstract, Lunar Planet. Sci. XXXIII (2002) (CD-ROM abstract 1877).
[69] S.J. Zhong, M.T. Zuber, L.-N. Moresi, Role of temperature-dependent viscosity and surface plates in spherical shell models of mantle convection, J. Geophys. Res. 105 (2000) 11063–11082.
[70] H. Lamb, Hydrodynamics, Dover, New York, 1945, p. 61.
[71] R.W. Griffiths, Thermals in extremely viscous fluids, including the effects of temperature-dependent viscosity, J. Fluid Mech. 166 (1986) 115–138.
[72] G. Schubert, V.S. Solomatov, P.J. Tackley, D.L. Turcotte, Mantle Convection and the thermal history of Venus, in: S.W. Bougher, D.M. Hunten, R.J. Phillips (Eds.), Venus II, Univ. of Ariz. Press, 1997, pp. 797–844.
[73] V. Steinbach, D.A. Yuen, The effects of multiple phase transitions on Venusian mantle convection, Geophys. Res. Lett. 19 (22) (1992) 2243–2246.
[74] K. Hirose, Phase transitions in pyrolitic mantle around 670-km depth: implications for upwelling of plumes from the lower mantle, J. Geophys. Res. 107 (B4) (2002).
[75] P. Olson, D.A. Yuen, Thermochemical plumes and mantle phase transitions, J. Geophys. Res. 87 (1982) 3993–4002.
[76] U.R. Christensen, D.A. Yuen, Layered convection induced by phase transitions, J. Geophys. Res. 90 (B12) (1985) 10291–10300.
[77] P. Machetel, P. Weber, Intermittent layered convection in a model mantle with an endothermic phase change at 670 km, Nature 350 (1991) 55–57.
[78] T. Nakakuki, H. Sato, H. Fujimoto, Interaction of the upwelling plume with the phase and chemical boundary at the 670 km discontinuity: effects of temperature-dependent viscosity, Earth Planet. Sci. Lett. 121 (1994) 369–385.
[79] P.J. Tackley, D.J. Stevenson, G.A. Glatzmeier, G. Schubert, Effects of an endothermic phase transition at 670 km depth in a spherical model of convection in the Earth's mantle, Nature 361 (1993) 699–704.
[80] J. Ita, S.D. King, Sensitivity of convection with an endothermic phase change to the form of governing equations, initial conditions, boundary conditions, and equation of state, J. Geophys. Res. 99 (1994) 15,919–15,938.
[81] A. Chopelas, R. Boehler, T. Ko, Thermodynamics and behavior of γ-Mg_2SiO_4 at high pressure: implications for Mg_2SiO_4 phase equilibrium, Phys. Chem. Miner. 21 (1994) 351–359.
[82] H.-P. Bunge, M.A. Richards, J.R. Baumgardner, Effect of depth-dependent viscosity on the planform of mantle convection, Nature 379 (1996) 436–438.
[83] A. Navrotsky, Thermodynamic properties of minerals, in Mineral Physics and Crystallography — a handbook of physical constants, AGU (1995) 18–28.